J. Chem. Sci. Vol. 129, No. 5, May 2017, pp. 589–599. © Indian Academy of Sciences.
DOI 10.1007/s12039-017-1269-3

REGULAR ARTICLE

Ammonia treated Mo/AC catalysts for CO hydrogenation with improved oxygenates selectivity

SHARIF F ZAMAN*, NAGARAJU PASUPULETY*, ABDULRAHIM A AL-ZAHRANI, MUHAMMAD A DAOUS, S S AL-SHAHRANI, HITOSHI INOKAWA, LACHEZAR A PETROV and HAFEDH DRISS

Chemical and Materials Engineering Department, Faculty of Engineering, King Abdulaziz University, P.O. Box 80204, Jeddah 21589, Saudi Arabia
E-mail: zfsharif@gmail.com; sfzaman@kau.edu.sa; pasupulety@gmail.com; nsampathrao@kau.edu.sa

MS received 25 December 2016; revised 21 March 2017; accepted 27 March 2017

Abstract. A series of ammonia treated Mo/Activated Carbon (AC) catalysts were synthesized by wet impregnation method by nominal incorporation of 5, 10 and 15 wt% of molybdenum. The calcined catalysts (500°C, 4 h, N_2 flow) were subjected to a stepwise ammonia treatment at temperatures from 25 up to 700°C. This work reports for the first time, ammonia treated different loadings of Mo on DARCO mesoporous activated carbon for CO hydrogenation reaction. These catalysts were tested in the reaction temperature range of 250–325°C, 7 MPa and 12000/h (GHSV for reactor volume 0.5 mL). At 250°C, all the catalysts showed total oxygenate selectivity of ~50%, mainly methanol. At 325°C, total oxygenate selectivity of 16.5% with 18% CO conversion was obtained on 10Mo-N/AC. The result of alcohol distribution revealed high selectivity to propanol (39%) over methanol (34%) at 325°C on 10Mo-N/AC which highlights its unique catalytic behavior in CO hydrogenation. Further, $10MoO_3$/AC catalyst, with no treatment of ammonia, showed only 4% of CO conversion with 96% hydrocarbon selectivity. Only 0.5% of CO conversion was observed on AC itself at 325°C. The improved oxygenates selectivity on 10Mo-N/AC was associated with $Mo^{\delta+}$ sites on AC generated *via* ammonolysis.

Keywords. Molybdenum nitride; activated carbon; CO hydrogenation; liquid oxygenates; ammonolysis.

1. Introduction

One of the most important challenges that mankind will face in the upcoming years, is to secure the needed energy supply for the increasing energy demand, while at the same time minimizing the negative environmental impact of mass energy production. Syngas utilization is one of the interesting alternative routes for producing liquid fuels and a variety of chemicals. Syngas can be produced from different carbon containing materials, such as coal, natural gas and biomass by means of gasification and reforming. Syngas can be converted into hydrocarbons, methanol and higher alcohols depending on the type of catalyst used and reaction conditions.

Higher alcohol synthesis (HAS) is an exothermic process and low temperature and high pressure favor the alcohol formation. The side reactions taking place are water gas shift and formation of hydrocarbons. Synthesized hydrocarbons usually are dominated by methane together with certain amount of other high molecular weight paraffins and olefins. Non-alcoholic oxygenated products such as aldehydes, esters and ethers are also produced depending on the type of the catalyst used and operating conditions.[1] A large number of published reports dealt with the preparation of oxygenates or hydrocarbons from syngas using bulk catalysts like Ni-Mo_2S,[1] Co-Mo_2S,[2] Mo_2C[3,4] and MoP.[1] Furthermore, Cu mixed Co catalysts were also extensively studied for HAS preparation from syngas.[5]

Supports like Activate Carbon (AC), Al_2O_3, SiO_2 and ZrO_2 have been studied for HAS by CO hydrogenation. The support effect strongly depends on the state of the active phase such as metal, oxide, and sulfide. Mo based catalysts with acidic supports such as Al_2O_3 and ZrO_2 were found to suppress the alcohol formation pathways and increased the hydrocarbon formation during CO hydrogenation.[6]

Activated carbon as a support shows some potential advantages such as large surface area, high thermal stability and low tendency of carbon deposition. Spreading the Mo active phase on a high surface area support was found to be advantageous as it increases the number of active sites due to improved dispersion and distribution.[7]

*For correspondence

Several studies were performed using activated carbon[8–10] and multi-walled carbon nanotubes (MWCNT),[11,12] as supports for MoS_2 that showed enhanced catalyst activity due to higher dispersion of the sulfide. K-promoted Ni-Mo catalysts supported on microporous activated carbon was used for syngas to HAS process by Liakaku *et al.*[13] Ma *et al.*,[14] studied the influence of acid treated AC as a support with K-Ni-Mo active phase for CO hydrogenation reaction. The K-Ni-Mo/AC catalyst was more selective to oxygenates (>40%, CO_2-free basis at 5 MPa and 265°C) over bulk K-Ni-Mo catalyst. The interaction of activated carbon with the Ni-Mo species prevents the complete reduction of the active metals (Ni^0 and Mo^0 lead to methane formation) and preserves partially oxidized Mo and Ni species, which are thought to be active sites for alcohol formation.[14] Zhang *et al.*,[15] synthesized Ni-Mo-K sulfide doped with 15% carbon nanotubes (CNT) and used for the syngas-to-HAS reaction. The authors concluded that CNT assists the hydrogen spillover to Ni-Mo-K surface and stabilizes the partially oxidized Ni-Mo species which led to higher alcohol formation.

Mesoporous AC, instead of microporous AC, have received much attention because of their relatively large pore size (>2nm) and uniform porosity which facilitate the reactant diffusion, increases the pore accessibility and improves the dispersion of supported active component by confining them in the well-defined pores.[16–18] Present work reports the first time, ammonia-treated different loadings of Mo on DARCO (trade mark for activated carbon derived from lignite and sold by ICI America, Inc., Wilmington, Delaware) mesoporous activated carbon (written as Mo-N/AC throughout this paper) for CO hydrogenation reaction. Further, the characteristics of the catalyst were established by BET-pore size distribution, CO and H_2-TPD, XPS and HR-TEM techniques.

2. Experimental

2.1 *Materials*

Ammonium heptamolybdate $(NH_4)_6Mo_7O_{24} \cdot 4H_2O$ (≥99.9%)) and DARCO mesoporous activated carbon (AC) with 20–40 mesh grain size were purchased from Sigma-Aldrich. The obtained AC was dried at 100°C for 12 h and used without any further purification. According to the AC manufacturer, it contains ≤12% moisture, dust ≤0.4% and mineral impurities (K, Si, Sn and Fe) <1%.

2.2 *Catalyst preparation*

Ammonium heptamolybdate equivalent to 5, 10 and 15 wt% of Mo was dissolved in 50 mL of deionized water and the resulting solution was continuously stirred for 1 h. To this solution, approximately 5 g of AC was added and the mixture was aged for 12 h. The excess water was evaporated using a hot plate. The resulting solids were dried overnight in a preheated oven at 100°C under static air. All the prepared catalysts were calcined at 500°C for 4 h under N_2 flow (30 mL/min). The calcined samples were subjected to stepwise temperature programmed ammonia treatment. One gram of the calcined sample was placed in a quartz reactor fitted with quartz frit. The nitridation procedure was as follows: In the first step, catalyst was kept at 120°C for 30 min under continuous He flow. In the second step, gaseous ammonia was introduced to the catalyst bed with an approximate flow rate of 400 mL/min and the reactor temperature was increased from 120 to 350°C with a ramping rate of 1°C/min. In the third step, the catalyst temperature was increased from 350 to 700°C with a ramping rate of 0.5°C/min and aged at this temperature for 2 h under continuous flow of ammonia. In the fourth step, the reactor was cooled down to room temperature under He flow at a rate of 30 mL/min. In the fifth step, the sample was passivated with 1 vol.% O_2-balanced He at a flow rate of 30 mL/min for 1 h.

These catalysts were denoted as 5Mo-N/AC, 10Mo-N/AC and 15Mo-N/AC. Herein, the prefix 5, 10 and 15 represent the weight percentage of molybdenum impregnated on activated carbon. Until unless stated, these samples were used for characterization studies. The catalyst with no treatment of gaseous ammonia with 10 wt% Mo loading was denoted as $10MoO_3/AC$.

2.3 *Catalyst characterization techniques*

The BET surface area and pore size distribution of the samples used in the present study were determined by a Quantachrome Nova Station adsorption equipment at liquid nitrogen temperature after outgassing the samples at 200°C under the flow of N_2 for 2 h.

The X-ray diffractograms of the samples used in the present study were obtained on a EQUINOX 1000 inel XRD instrument using Co K_α = 1.7902 Å, X-ray source generator settings at 40 kV and 30 mA with real time acquisition over 110° of 2θ. The FTIR analysis of Mo-N/AC samples was performed on a Bruker Vertex 70/70v FTIR spectrometer using KBr pellet method. Transmission electron microscopy (TEM) images and high resolution TEM images and energy dispersive X-ray analysis (EDS) of Mo-N/AC samples were collected on Technai 200 kV D1234 Super Twin microscope with camera length of 97 cm.

XPS results of Mo-N/AC samples were collected on a SPECS GmbH high vacuum multi-technique surface analysis system equipped with Mg K α 1253.6 eV X-ray source. Temperature programmed desorption (TPD) analysis of Mo-N/AC samples were determined using adsorption-desorption of CO and H_2 with Quantachrome pulsar automated chemisorption instrument. All gases were supplied by Abdulla Hashim Gas (AHG), Saudi Arabia, and certified concentration (14.95% CO-He and 99.99% H_2) was used as a probe gas. In a typical

experiment, approximately 0.1 g of catalyst was pretreated in He gas flow (10 mL/min) at 200°C for 1 h followed by hydrogen treatment at 400°C for 4 h. Subsequently, the catalyst was brought to room temperature under the flow of He and saturated with probe gas (either CO or H_2). Desorption of probe gas was performed after 1 h of He flushing over a temperature range of 30–400°C at a ramping rate of 10°C/min.

2.4 *Catalytic activity tests*

Catalytic activity tests were performed using PID Eng and Tech system (Spain) equipped with a flow microreactor, mass flow, pressure and temperature controllers. The mixture of CO:H_2 = 1:1 volume ratio was selected as model feed at 12000/h (reactor volume 0.5 mL) GHSV (gas hourly space velocity). Catalytic activity tests were carried out in the temperature range of 250–325°C with 25°C step size at the applied pressure of 7 MPa. All the gases for the catalytic activity tests were supplied by Abdulla Hashim Gas (AHG), Saudi Arabia.

For example, 500 mg of Mo-N/AC catalyst was loaded in to a copper lined stainless steel tube reactor (inside diameter 6.35 mm and length 9.53 mm) diluted with equal amount of quartz beads was treated with H_2 flow of 50 mL/min at 500°C for 2 h. Subsequently, the H_2 flow was replaced by N_2 and reactor temperature was brought back to 250°C. The reactant gas mixture CO:H_2 = 1:1 volume ratio was introduced with flow rate of 100 mL/min through an activated carbon trap (which traps iron carbonyls formed inside the gas tank) into the reactor to attain the required pressure. After attaining the steady state at a set temperature and pressure of the reaction, the reactor exit stream was directed through a heated line at 160°C to Agilent 7890A GC equipped with TCD connected with Restek Plot Q column for CO and CO_2 separation and to flame ionization detector (FID) fitted with HP Plot Q column for separation of hydrocarbons (methane, ethane, ethylene, propane, propylene and butane) and oxygenates (methanol, ethanol, propanol, butanol, acetone, acetic acid, acetaldehyde and ethyl acetate) estimation. Acetone, acetic acid, acetaldehyde and ethyl acetate are reported as other oxygenates in the activity results. At each temperature, five experimental points were collected and the results were reproducible within the error of ±0.1%. The same catalyst load was used for the tests at the three reaction temperatures. Negligible (<0.1%) CO conversion was found on empty SS copper lined reactor under identical reaction conditions. The syngas conversion and selectivity of the products were calculated by the following equations:

$$CO\ conversion\ (mass\ \%) = \frac{CO\ initial\ moles - CO\ final\ moles}{CO\ initial\ moles} \times 100$$

$$Selectivity\ (mass\%) = \frac{n_i C_i\ prodcut}{\sum n_i C_i} \times 100$$

where, n_i is the number the carbon atoms in the molecule of the ith component and C_i is the mole fraction of ith component in the reaction mixture at the reactor exit.

3. Results and Discussion

3.1 *BET surface area and pore size distribution studies*

Figure 1a shows the physorption isotherms of activated carbon (AC) and Mo-N/AC samples. The AC and Mo-N/AC exhibited type-II Brunauer-Deming-Deming-Teller isotherms typical for mesoporous solids.[19] Adsorption hysteresis was reported due to multilayer physorption isotherms usually associated with capillary condensation in mesopores. In the present study, *H*4 type hysteresis loops were observed, which were associated with narrow slit-like pores in all the samples.[20] Furthermore, in Mo-N/AC samples, capillary condensation of adsorbate N_2 in the pores occurred at a lower relative pressure than that of AC under similar physorption conditions (catalyst 200 mg and 200°C, 2 h, N_2 pretreatment), which is indicative of reduction in the pore size of AC in Mo-N/AC samples. This might be

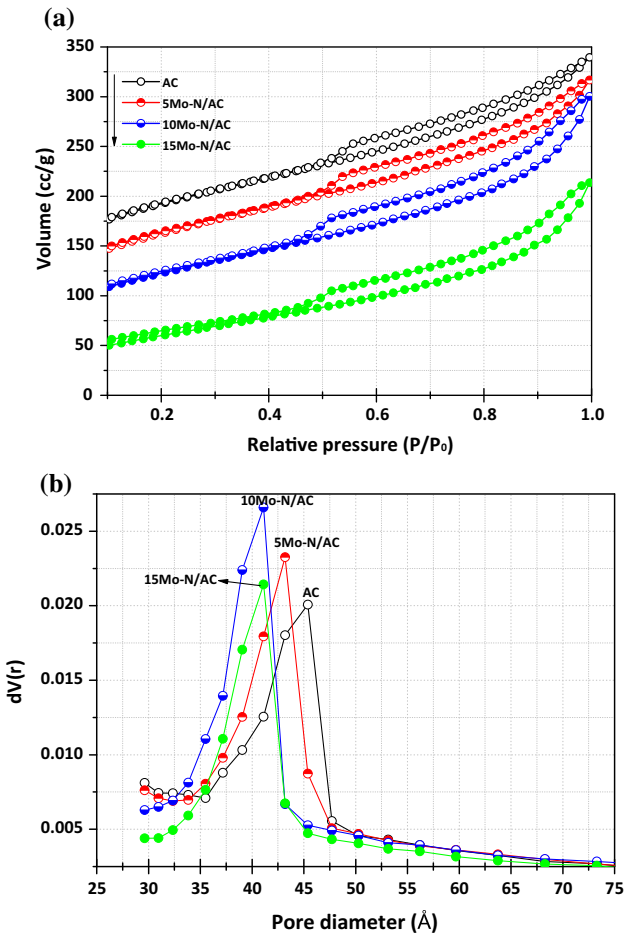

Figure 1. (**a**) BET isotherms; (**b**) pore size distribution in terms of derivative expression of pore volume with pore size between r and r+dr for samples AC and Mo-N/AC.

associated with the location of Mo in the mesopores of AC with Mo loadings.

Figure 1b presents the BJH pore size distribution of AC and Mo-N/AC samples. Unimodal mesopore distribution was observed in all these samples with the pore diameter range of 30 − 50 Å. The AC showed mesoporous texture in the range of 35 − 50 Å and averaged at 45 Å. On the other hand, Mo-N/AC samples showed a shift in the mesopore average diameter to lower side (Figure 1a hysteresis loop was shifted to lower P/P_0). For instance, 5Mo-N/AC showed mesopores in the range of 34–47.5 Å and averaged at 43 Å and 10- and 15Mo-N/AC samples showed mesopores in the range of 32–45.0 Å and averaged at 41.0 Å. The results indicate that the mesopores distribution in a wide range in support AC, whereas, partial filling of AC pores by Mo component narrowed the diameter range of mespores in Mo-N/AC samples. Further, at 15wt.% of Mo loading, AC showed reduced volume of mesopores compared to 10Mo-N/AC sample which suggests, to some extent, that mesopores were filled totally by Mo species at this loading of Mo (Figure 1b, line with filled circle). Champson *et al.*,[21] also reported reduction of BET surface area and pore volume for temperature programmed ammonia treated 10Mo-N/AC (DARCO) catalyst over its support. The authors related that the reduction of pore volume and BET surface area was due to Mo-N formation inside the mesopores of AC. In this study, the systematic transformation of mesopore diameter to narrow size upon Mo loading on AC was associated with stepwise temperature programmed ammonia treatment, which resulted in the formation of Mo-N species in the mesopores of AC.

The AC showed the BET surface area and mesopore volume as 609.0 m^2/g and 0.460 mL/g,respectively. On the other hand, the BET surface area and mesopore volume for 5-, 10- and 15Mo-N/AC samples obtained as 561.0, 486.0 and 218 m^2/g and 0.449, 0.420 and 0.297 mL/g, respectively. The decrease in the volume of mesopores was associated with partial filling of AC mesopores with Mo-N species. Despite the pore filling, the integrity of mesopore structure of AC in Mo-N/AC was intact, as observed by the N_2 sorption isotherms.

3.2 *XRD analysis*

XRD spectra of AC and Mo-N/AC samples are presented in Figure S1 (Supplementary Information). Support (AC) related X-ray reflections are pronounced at 2θ = 22.0, 24.0, 31.2, 42.8, 44.5, 46.25, 49.9, 52.0, 59.0, 71.0, 76.0, 81.0 and 98.0° which are attributed to activated carbon graphene framework. Identical reflections were pronounced at similar 2θ values due to the support in Mo-N/AC samples. No XRD reflections were observed for Mo phases up to 15 wt% of Mo loading on AC. No crystalline phases of molybdenum were detected for 10 wt% of Mo on Norit activated carbon catalysts and attributed to a high degree of dispersion of the Mo phase on the support.[22] However, in the present study, the intensity of the AC related X-ray reflections were decreased for samples from 5Mo-N/AC to 15Mo-N/AC under identical XRD conditions (30 mg catalyst, 2 h analysis). This phenomenon was likely due to interactions of Mo species with activated carbon graphite structure. The results suggest that the Mo-related crystallites are $\leq$ 4 nm, and/or distributed well on the surface of the support.

3.3 *FTIR studies*

FTIR studies were performed to determine the changes on the surface carbon-oxygen functional groups with Mo loading in Mo-N/AC samples and the results are presented in Figure S2 (Supplementary Information). The FTIR spectra of AC exhibited major bands in the fingerprint region (400–1500 cm^{-1}) and minor bands in the functional group region (4000–1500 cm^{-1}). The broad band in the region of 950–1300 cm^{-1}(centered at 1100 cm^{-1}) is ascribed to C-O stretching vibration, such as those in ethers, phenols and hydroxyl groups.[23] The weak bands observed at 700 and 780–800 cm^{-1} are attributed to out-of-plane O-H bending and out-of-plane = C-H bending vibrations, respectively. The presence of 1580 cm^{-1} stretching vibration reveals the carbonyl functional groups (C=O) on AC. The band appearing around 3400 cm^{-1} is ascribed to O-H stretching vibration of carboxylic acid or physically adsorbed water. Similar bands are pronounced in the region of 950–1300 and 700–800 cm^{-1} for Mo-N/AC samples, which indicate the intact AC surface functional groups even after Mo impregnation and ammonolysis process. In addition, new bands appeared at 900, 1400 and 3100 cm^{-1} in Mo-N/AC samples. The bands at 900 and 3100 cm^{-1} are ascribed to C-H vibrations in aromatic carbon structures.[23] The appearance of these bands after the impregnation of Mo on AC might be associated with the formation of C-H bonds in aromatic rings, as a consequence of the opening of cyclic ether bridges by the interaction of molybdenum species with ether groups[23] or hydrogenation of sp^2 carbon during the ammonolysis process. The band at 1400 cm^{-1} is related to deformational vibration of physically adsorbed water.[24]

The decrease in the infrared intensity of carboxyl or conjugated carbonyl groups at 1720 cm^{-1} in 15Mo-N/AC was related to the interaction between molybdenum species with carboxyl or conjugated carbonyl

groups.[25] In the present study, more prominent C-O vibration was observed on AC at 1100 cm^{-1}. However, the intensity of this band was relatively decreased with increase of the Mo loading in Mo-N/AC samples. The result suggests C-O groups are chemical anchoring centers for the studied Mo-N/AC samples which led to Mo-O-C type of complexes in agreement with XPS data where C-O signal was grown with increasing of the Mo loading.

3.4 *XPS measurements*

Figure S3 (Supplementary Information) presents C 1*s*, O 1*s* and Mo 3*d* XPS patterns for AC and Mo-N/AC samples. The AC itself showed broad pattern for C 1*s* and the satellite bands in the binding energy range of 282.0–293.0 eV are attributed to different types of oxygen containing functional groups on AC surface. The Shirley deconvolution of C 1*s* yielded six chemically-shifted signals as shown in Figure S3. The C 1*s* peak centered at 284.6 eV is ascribed to sp^3 carbon of AC as the major component. The peak at relatively lower binding energy (283.7 eV) is endorsed to C=C (sp^2 carbon) which suggests the presence of unoxidized domains in AC. Additionally, four more carbon-related components exist at 285.5, 287.0, 289.5 and 291.0 eV. They are assigned to -C-O, carbonyl (-C=O), carboxylate ($^{-}$O-C=O) and carboxyl (-COOH) functionalities, respectively.[26] Identical components, pronounced due to C 1*s* in Mo-N/AC samples (Figure S3), indicate that all characteristic functional groups of C 1*s* remained intact, even after Mo was impregnated on AC. However, the changes observed in Mo-N/AC samples with respect to Mo loading are as follows: (i) The intensity of C-C peak was reduced and a prominent XPS tail (around 285.5 eV) appeared from AC to 15Mo-N/AC which indicates possible interactions exist between surface Mo and AC functional groups. (ii) In particular, relatively intensified -C-O and -C=O bands with respect to Mo loading indicates the presence of the interaction between the surface Mo atoms and these functional groups through delocalization of electrons.

O 1*s* XPS pattern of AC and Mo-N/AC samples are presented in Figure S3. The Shirley deconvolution of O 1*s* yields four different components in the binding energy range of 528-540 eV. The peak centered at 532.8 eV is attributed to carbonyl oxygen (C=O). The peaks registered at 534.0 and 535.2 eV are ascribed to hydroxyl oxygen (C-OH) and carboxylate/carboxyl oxygen, respectively.[19] The peak centered at 530.8 eV suggests the presence of lattice oxygen in O-Mo species.

Furthermore, Figure S4 (Supplementary Information) shows that the Mo 3*d* peaks are pronounced at 232.6 and 235.7 eV due to the split components of $3d_{5/2}$ and $3d_{3/2}$, respectively. The existence of these bands suggests that the Mo^{6+} valence state is present in all the studied catalysts.[21] The surface molybdenum content (atomic %) on 5Mo-N/AC, 10Mo-N/AC and 15Mo-N/AC was found to be 0.40, 0.70 and 0.82 atomic percentage, respectively.

3.4a *CO-TPD studies*: CO-TPD results of reduced AC and Mo-N/AC samples are presented in Figure 2a. No CO sorption was observed on AC. On the other hand, a single desorption signal was observed in all the studied Mo/AC samples. On 5- and 15Mo-N/AC, CO desorption peak maximum was observed at 165°C with a capacity of 45 and 50 μ mol/g, respectively. However, for 10 Mo-N/AC, CO desorption peak maximum was observed at 200°C with a capacity of 100μmol/g. These results indicate that CO sorption is relatively higher at 10 wt% of Mo loading over 5 and 15 wt%. This is associated with homogeneous distribution of Mo species at this loading on AC, as observed by TEM analysis. Three types of CO sorptions were reported on Mo/Al_2O_3 surface:[27] (i) physically adsorbed CO in the temperature range of 25 − 80°C; (ii) molecular CO adsorption in the temperature range of 100 − 300°C; and (iii) dissociative CO adsorption in the temperature range of 600 − 1000°C[28]. Bulk Mo_2N displayed two CO desorption peaks at 165 and 300°C. The first CO desorption peak was assigned to desorption of molecularly adsorbed CO on $Mo^{\delta+}$ (Mo^{2+} and Mo^{3+}) sites (Mo-C ≡ O). The later CO desorption peak was assigned to desorption of NCO species.[29] In this study, all the Mo-N/AC samples displayed molecular CO desorption peaks with maxima in the range of 150–200°C with different CO desorption capacities. According to Miura *et al.,*[28] molecular CO desorption can be enhanced by the surface modification of Mo species. The CO-TPD result reveals CO sorption on $Mo^{+\delta}$ sites present on AC in Mo-N/AC samples.

3.4b *H_2 -TPD studies*: H_2-TPD results of Mo-N/AC samples are presented in Figure 2b. A single desorption signal characterized by several humps were observed in the temperature range of 150–350°C in all Mo-N/AC samples. Hydrogen desorption from Mo (100) surface was reported to happen at room temperature.[27] It was accepted that the hump-like profile was the result from either reversible adsorption of $H_2$and/or simultaneous H_2 desorption from the Mo/AC surface. The maximum H_2 desorption of 60 μmol/g was observed at 10Mo-N/AC compared to 5- and 15Mo-N/AC samples. Hence, the decreasing order of H_2 desorption is as follows: 10Mo-N/AC (60 μmol/g) > 15Mo-N/AC (26 μmol/g) > 5Mo-N/AC (17 μ mol/g). The result

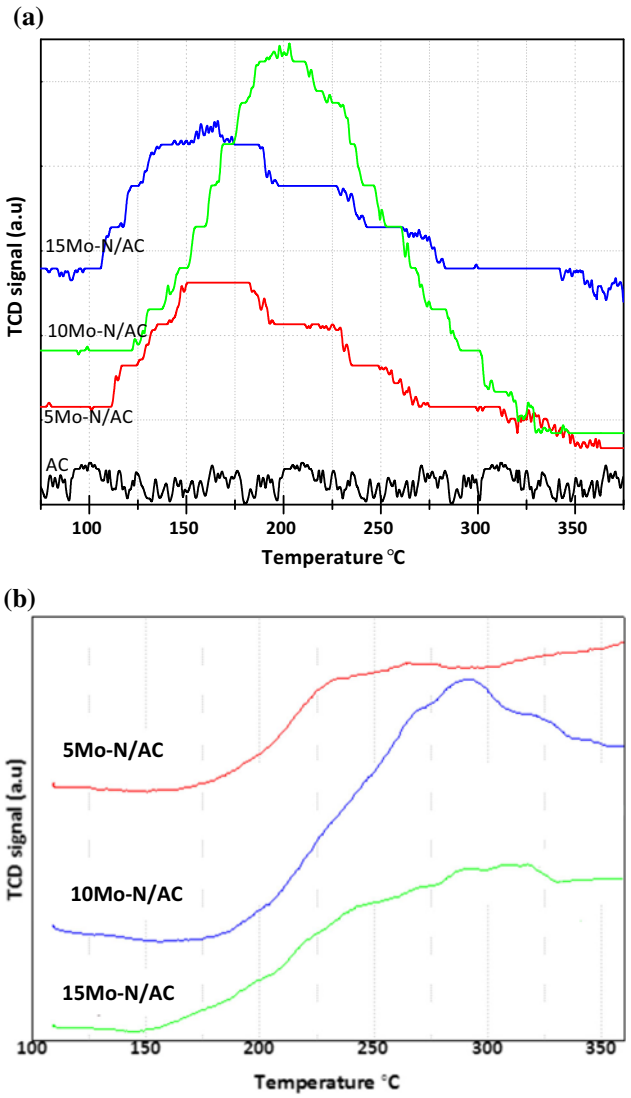

Figure 2. (**a**) CO-TPD results of AC and Mo-N/AC samples in terms of thermal conductivity signal (a. u.). (**b**) H_2-TPD results.

indicates that the CO was preferentially adsorbed on Mo species rather than hydrogen.

3.5 *TEM studies*

The TEM images of AC and Mo-N/AC samples are presented in Figure S5 (Supplementary Information). The wrinkle-folded morphology was observed for AC (Figure S5(a)), which is attributed to the carbon in sp^3 hybridization in C-C and or C-O links.[30] The morphology of the carbon changed upon Mo loading and appears as nebulous type. The Mo spherical particles (marked with circle) are distributed on the AC with the size range of 1–3 nm. The large sized (≈4 nm) Mo particles on AC were observed at 15% loading (Figure S5(d)) which suggest aggregation of Mo particles. Usually, Mo species agglomerate because of the electrostatic attractions between anionic part of one unit and counter cationic part of the other unit.[30] Mo content by EDS analysis for 5-, 10- and 15 Mo-N/AC samples were found to be 4.8, 9.5 and 14.0 wt%, respectively, which agree with the nominal loading of the Mo metal at the impregnation step.

The high resolution TEM images of 10Mo-N/AC sample are presented in Figure S6 (Supplementary Information). Well-distributed Mo particles (marked with circles in Figure S6(a)) are observed in the wrinkled channels of AC. The Mo particles are sized in the range of 1-2 nm. The d-spacing line profile of Mo particle is presented in Figure S6 (b). The d-spacing of channels (0.144 nm) is consistent with the plane (062) of orthorhombic molybdenum trioxide [00-005-0508]. These results are in agreement with XPS data where Mo^{6+} valence state is observed.

In present work, ammonia treated sample characterization exhibited oxide form of Mo. This might be associated with quick conversion of nanosized Mo-N particles (≤4 nm) to oxide under X-ray or electron beam exposure and or due to catalyst exposure to atmospheric air during the characterization. For this reason, we performed the catalytic activity test on ammonia-gas-untreated MoO_3/AC catalyst for this reaction. In the following section, activity results reveal that the catalytic behavior of Mo-N/AC is different in fair amount, in both conversion and selectivity, when compared with those of MoO_3/AC catalyst.

3.6 *Catalytic activity*

The CO hydrogenation activity results on the prepared catalysts are presented in Figure 3. The catalytic activity tests were performed in the temperature range of 250–325°C, 7.0 MPa and 12000/h GHSV (reactor volume 0.5 mL). Catalytic activity of the support was also studied under similar reaction conditions. Only, <0.5% CO conversion was observed on AC at 325°C. On the other hand, maximum CO conversion of 18.0% was observed on 10Mo-N/AC compared to 5Mo-N/AC (9.5%) and 15Mo-N/AC (13.5%) at 325°C. The result suggests inadequate amount of Mo active surface at 5% Mo loaded sample, and at 15% Mo loading, aggregation of Mo species leads to low catalytic activity. Hence, 10% Mo loading was found to be optimal for AC for CO hydrogenation reaction. Further, CO conversion was increased with an increase in the reaction temperature. Hydrocarbon selectivity was increased with an increase in the reaction temperature for all the Mo-N/AC catalysts. Higher temperature is favorable for the formation of hydrocarbons and CO_2 *via* water gas shift reaction. The higher hydrocarbon formation can also be

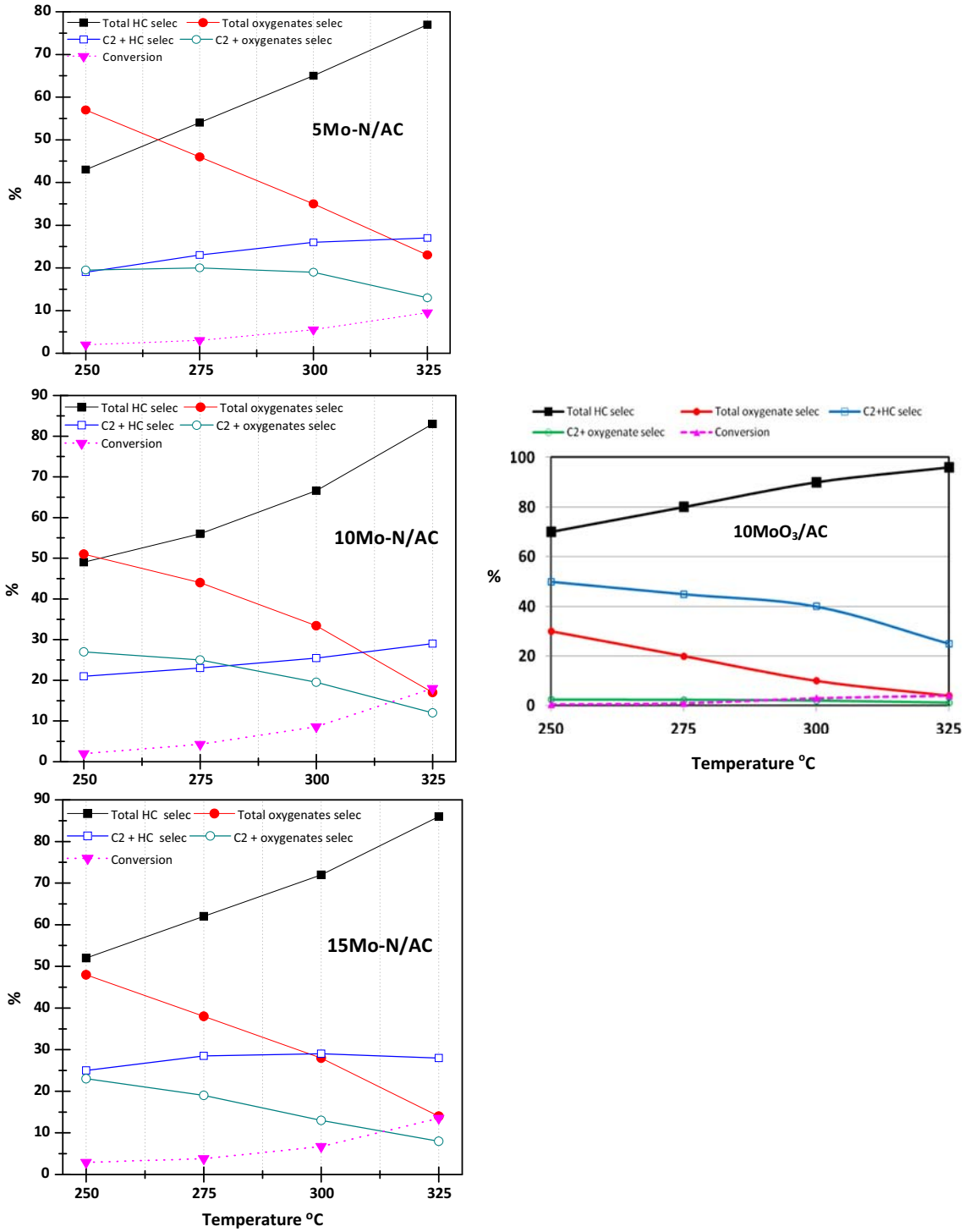

Figure 3. CO hydrogenation activity on Mo/AC catalysts at reaction temperature 250–325°C, 7MPa and GHSV 12000/h (reactor volume 0.5 mL).

related to the hydrogenation of carbonaceous intermediates ($-C_xH_Y$) rather CO insertion into it.[29] Furthermore, the increased CO_2 concentration at higher temperatures can also alter the CO/H_2 ratio in the reactor zone and influence the CO insertion process followed by higher alcohol formation. In the present work, increased hydrocarbon selectivity with increased CO conversion with respect to reaction temperature suggests higher hydrogenation tendency of these catalysts.

On the other hand, the total oxygenates selectivity decreased with increase in the reaction temperature. The studied Mo-N/AC catalysts showed maximum oxygenates selectivity, ~50%, CO_2-free basis, mainly methanol in the liquid product, at 250°C, however, with

a low CO conversion (~2.0%). At 300°C, a reasonable CO conversion of 5.5, 8.6 and 6.7%, with a reasonable total oxygenate selectivity of 30, 35 and 28% were observed on 5-, 10- and 15 Mo-N/AC catalysts, respectively.

Catalysts, respectively. Further, oxygenates selectivity of 21% with 9.5% CO conversion was obtained on 5Mo-N/AC, whereas, around 14% of both oxygenates selectivity and CO conversion was observed on 15Mo-N/AC at 325°C. Around 16.5% of total oxygenates selectivity with 18% CO conversion was obtained on 10Mo-N/AC at 325°C. Decrease in oxygenate selectivity was compensated by the increase in hydrocarbons, especially methane. Also C_2^+ hydrocarbon selectivity increased with reaction temperature suggesting an increase in hydrogenation capacity of Mo-N/AC catalyst at higher temperatures, *i.e.*, hydrogenation of liquid oxygenates to produce the corresponding hydrocarbons.

The catalytic activity of $10MoO_3/AC$ (without ammonia treated catalyst) was also studied under similar reaction conditions and the results are compared with 10Mo-N/AC catalyst. Only 4% of CO conversion, with 96% hydrocarbon and 4% oxygenate selectivity, was observed on $10MoO_3$/AC at 325°C. The $10MoO_3/AC$ catalyst has exhibited considerable amount of methanol with very little amounts of ethanol, propanol and other oxygenates in the liquid product distribution. On the other hand, oxygenates selectivity was significantly improved to 16.5% on 10Mo-N/AC catalyst at 325°C. However, on $10MoO_3/AC$ catalyst also at lower reaction temperature (250°C), maximum oxygenates selectivity of 30% with 0.5% CO conversion was observed. These results suggest that improved oxygenates selectivity due to ammonia treatment might be associated with $Mo^{\delta+}$ sites of Mo-N/AC catalysts. The results are in agreement with our CO-TPD data where, molecular CO adsorption take place on $Mo^{\delta+}$ sites.

Li *et al.*,[31] reported 36% CO conversion with 99% hydrocarbon selectivity on 18Mo/AC (not treated with gaseous form of ammonia) catalyst at 325°C, 5 MPa and GHSV 6 m^3/h/kg. Hydrocarbon formation, particularly methane formation, in CO hydrogenation using Mo based catalysts was reported in the following order: Mo metal (Mo^0) > Mo_2N ($Mo^{\delta+}$) > MoO_2(Mo^{4+}) > MoO_3(Mo^{6+}).[32] The decrease in the CO conversion on $10MoO_3/AC$ catalyst is associated with the bulk presence of the higher oxidation state molybdenum oxide sites.

3.7 *Alcohol distribution*

The results of alcohol distribution in the temperature range of 250–325°C on Mo-N/AC catalysts are presented in Figure 4. It is obvious from the results that methanol was the major alcohol produced on all the studied Mo-N/AC catalysts at temperatures up to 300°C. Further, methanol selectivity decreased with increase in the reaction temperature. At the same time, improved C_2^+ alcohol selectivity indicates that methanol homologation/ CO insertion to $-C_xH_y$ intermediate to chain propagation, was the additional reaction route leading to C_2^+ alcohol formation.

This phenomenon was intensified at 325°C particularly on the catalysts having 10 and 15 wt% Mo. Interestingly, propanol was the second highest selective compound in the alcohol distribution after methanol in all the cases, except on 10Mo-N/AC at 325°C. Further, selectivity of propanol (39%) was greater than that of methanol (34 %) and ethanol (13.5%) on10Mo-N/AC at 325°C. Butanol selectivity for all the cases was less than 3%. It is obvious from the alcohol distribution results that Mo-N/AC catalyst has some unique characteristics for showing high selectivity to C_3 alcohol. Getting high selectivity to propanol is very interesting and a new phenomenon, as according to Anderson-Schulz-Flory (ASF) distribution, the chain propagation should continue to high selectivity to the bulky end product, *i.e.*, butanol. Somehow, the chain propagation was ceased after formation of C_3 alcohol on Mo-N/AC catalysts. Further study is under progress to assess the effect of alkali metals on the catalyst.

The selectivity (CO_2 free) of ethanol and propanol in alcohol products together at 325°C decreased in the following order: 10Mo-N/AC (52.5%) > 15Mo-N/AC (43.5%) > 5Mo-N/AC (33%). The greater C_2^+ alcohol selectivity on 10Mo-N/AC was associated with higher adsorption capacity for CO and H_2. Miura *et al.*,[28] also reported that CO hydrogenation selectivity depends on CO chemisorption capacity of bulk MoO_3 and molybdophosphoric acids. The other oxygenates selectivity also increased with increase in the reaction temperature on these catalysts.

3.8 *Influence of support properties and Mo loading on the oxygenates formation*

In the present study, the AC contains small portion of surface acidic groups as evidenced by XPS/FTIR analysis. It is well-known that acidic supports such as Al_2O_3 and ZrO_2 suppress the formation of alcohols and increase the hydrocarbon formation on pre-reduced Mo catalysts. The present DARCO AC contains mostly sp^3 hybridized carbon atoms and C-O (ethers and phenol) functional groups with mesopores, which provide suitable interaction conditions between Mo and AC sur-

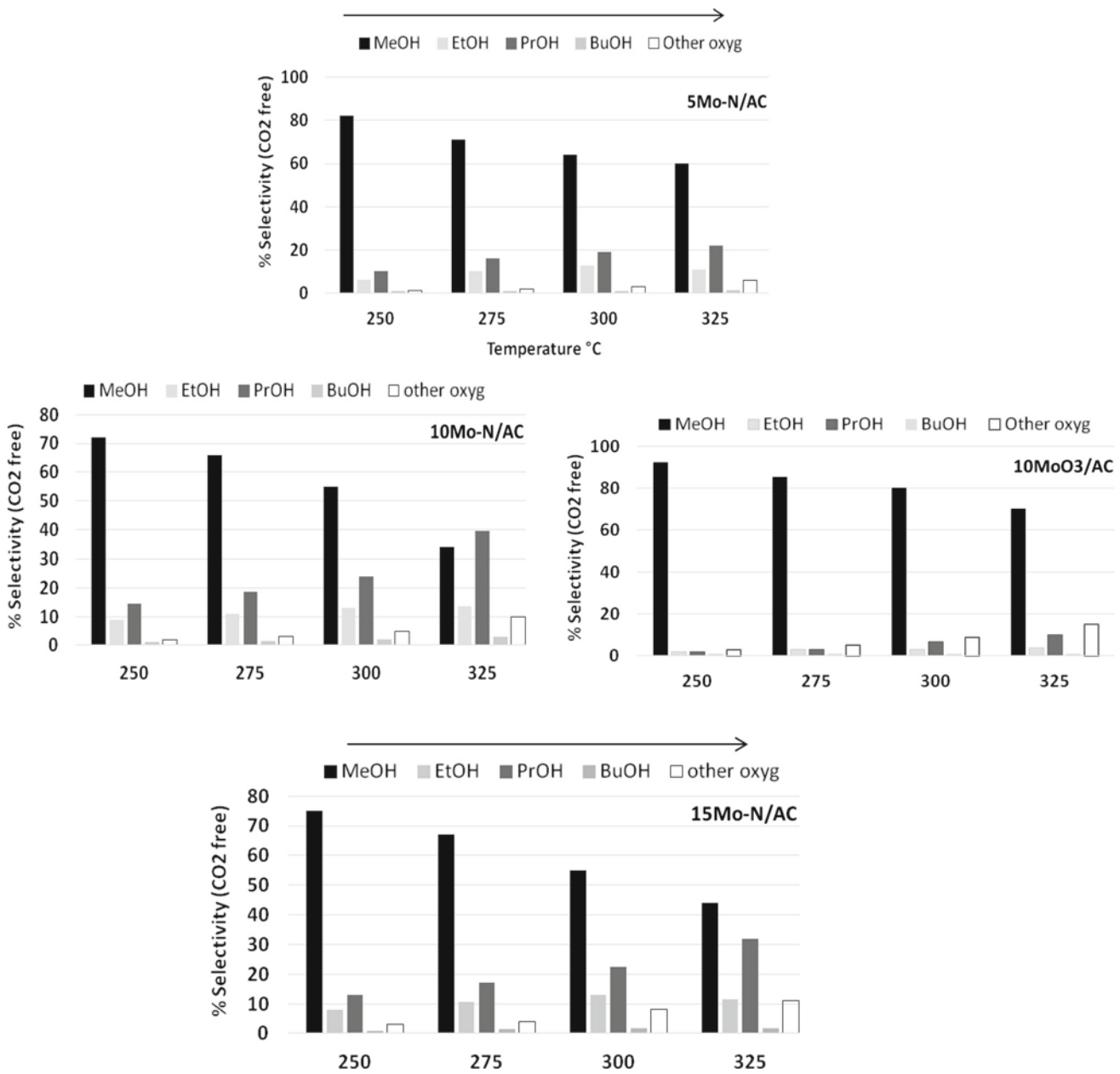

Figure 4. Alcohol distribution on Mo/AC catalysts in the temperature range of 250–325°C, 7 MPa and GHSV 12000/h (reactor volume 0.5 mL).

face. FTIR analysis of the spent AC and Mo-N/AC catalysts are presented in Figure S7 (a) (Supplementary Information). The sample exhibited identical bands as fresh catalysts in the finger print region of 400–1500 cm^{-1} and in the functional group region (4000–1500 cm^{-1}). In addition, new bands appeared at 2850 and 2920 cm^{-1} for all the spent catalysts. They are attributed to C-H vibration of hydrocarbons present on the surface of Mo/AC catalysts. The results of XPS measurements of the spent 10Mo-N/AC catalyst shows (Figure S7 (b)) the relatively increased C-O functional group of AC over its fresh counterpart, which reveals that Mo mobilization from C-O-Mo complex to the mesopores of AC during the CO hydrogenation. It is obvious from the spent catalyst analysis that the employed DARCO AC is stable at 325°C and 7 MPa.

4. Conclusions

Mo-N/AC catalyst showed interesting product selectivity, especially to alcohols ($C_1 - C_3$), for CO hydrogenation reaction. This is associated with $Mo^{\delta+}$ sites present on AC as revealed by CO-TPD studies. Among the Mo-N/AC catalysts, 10Mo-N/AC was found to be the most promising catalyst for CO hydrogenation to hydrocar-

bons and oxygenates due to high affinity for molecular CO adsorption and insertion into $-C_xH_y$. High selectivity to propanol, 39% over 34% for methanol, in alcohol distribution highlights the unique catalytic behavior of 10Mo-N/AC for CO hydrogenation reaction at 325°C.

The $10MoO_3$/AC catalyst, with no treatment of ammonia, showed only 4% of CO conversion and 96% hydrocarbon selectivity. These results suggest that improved oxygenates selectivity is associated with ammonia treatment which led to $Mo^{\delta+}$ sites. Our group is performing experiments to assess the effect of alkali metal on 10Mo-N/AC catalyst for CO hydrogenation reaction.

Supplementary Information (SI)

The XRD, FTIR, XPS, TEM, HR-TEM of fresh catalyst, Figures S1–S6 and FTIR, XPS of spent catalyst, Figures S7 are presented in Supplementary Information, available at www.ias.ac.in/chemsci.

Acknowledgements

This project was funded by the National Plan for Science, Technology and Innovation (MAARIFAH)-King Abdulaziz City for Science and Technology, the Kingdom of Saudi Arabia, (Award Number 12-PET2720-03). The authors acknowledge technical support with thanks Science and Technology Unit, King Abdulaziz University.

References

1. Zaman S and Smith K J 2012 A Review of Molybdenum Catalysts for Synthesis Gas Conversion to Alcohols: Catalysts, Mechanisms and Kinetics *Catal. Rev. Sci. Eng.* **54** 41
2. Paris R S, Montes V, Boutonnet M and Jaras S 2015 Higher Alcohol Synthesis over Nickel-Modified Alkali-doped Molybdenum Sulfide Catalysts Prepared by Conventional Coprecipitation and Coprecipitation in Microemulsions *Catal. Today* **258** 294
3. Iranmahboob J, Toghiani H and Hill D 2003 Dispersion of Alkali on the Surface of Co-MoS_2/Clay Catalyst: A Comparison of K and Cs as a Promoter for Synthesis of Alcohol *Appl. Catal. A: Gen.* **247** 207
4. Liakakou E T and Heracleous E 2016 Transition Metal Promoted K/Mo_2C as Efficient Catalysts for CO Hydrogenation to Higher Alcohols *Catal. Sci Technol.* **6** 1106
5. Lee J H, Hariprasad Reddy K, Jung J S and Yang E -H 2014 Role of Support on Higher Alcohol Synthesis from Syngas *Appl. Catal. A: Gen.* **480** 128
6. Surisetty V R, Dalai A K and Kozinski J 2011 Alcohols as Alternative Fuels: An Overview *Appl. Catal. A: Gen.* **404** 1
7. Duchet J C, Vanoers E M, Debeer V H J and Prins R 1983 Carbon-supported Sulfide Catalysts *J. Catal.* **80** 386
8. Gang L, Chengfang Z, Yanqing C, Zhibin Z, Yianhui N, Linjun C and Fong Y 1997 Synthesis of Mixed Alcohols from CO_2 Contained Syngas on Supported Molybdenum Sulfide Catalysts *Appl. Catal. A* **150** 243
9. Iranmahboob J and Hill D 2002 Alcohol Synthesis from Syngas over K_2CO_3/CoS/MoS_2 on Activated Carbon *Catal. Lett.* **78** 49
10. Li Z R, Fu Y L, Jiang M, Hu T D, Liu T and Xie Y N 2001 Active Carbon Supported Mo–K Catalysts Used for Alcohol Synthesis *J. Catal.* **199** 155
11. Ma X, Lin G and Zhang H 2006 Co-Mo-K Sulfide-Based Catalyst Promoted by Multiwalled Carbon Nanotubes for Higher Alcohol Synthesis from Syngas *Chin. J. Catal.* **27** 1019
12. Surisetty V R, Dalai A K and Kozinski J 2010 Alkali-Promoted Trimetallic Co-Rh-Mo Sulfide Catalysts for Higher Alcohols Synthesis from Synthesis Gas: Comparison of MWCNT and Activated Carbon Supports *Ind. Eng. Chem. Res.* **49** 6956
13. Liakakou E T, Heracleous E, Triantafyllids K S and Lemonidou A A 2015 K-promoted NiMo Catalysts Supported on Activated Carbon for the Hydrogenation Reaction of CO to Higher Alcohols: Effect of Support and Active Metal *Appl. Catal. B: Environ.* **165** 296
14. Ma C-H, Li H-Y and Lin G-D 2010 MWCNT-Supported Ni–Mo–K Catalyst for Higher Alcohol Synthesis from Syngas *Catal. Lett.* **137** 171
15. Wang J-J, Xie J-R, Huang Y-H, Chen B-H, Lin G-D and Zhang H-B 2013 An Efficient Ni–Mo–K Sulfide Catalyst Doped with CNTs for Conversion of Syngas to Ethanol and Higher Alcohols *Appl. Catal. A: Gen.* **468** 44
16. Shao Y, Xu Z, Wan H, Chen H, Zheng S and Zhu D 2011 Enhanced Liquid Phase Catalytic Hydrodechlorination of 2,4-dichlorophenol over Mesoporous Carbon Supported Pd Catalysts *Catal. Commun.* **12** 1405
17. Zhang Y, Wang A and Zhang T 2010 A New 3D Mesoporous Carbon Replicated from Commercial Silica as a Catalyst Support for Direct Conversion of Cellulose into Ethylene Glycol *Chem. Commun.* **46** 862
18. Hussain M and Ihm S-K 2009 Synthesis, Characterization, and Hydrodesulfurization Activity of New Mesoporous Carbon Supported Transition Metal Sulfide Catalysts *Ind. Eng. Chem. Res.* **48** 698
19. Strzemiecka B, Voelkel A, Donate-Robles J and Martin-Martinez J M 2014 Assessment of the Surface Chemistry of Carbon Blacks by TGA-MS, XPS and Inverse Gas Chromatography Using Statistical Chemometric Analysis *Appl. Surf. Sci.* **316** 315
20. Sing K S W, Everett D H, Haul R A W, Moscou L, Pierotti R A, Rouquerol J and Siemieniewska T 1985 Reporting Physorption Data for Gas/Solid Systems with Special Reference to the Determination of Surface Area and Porosity *Pure Appl. Chem.* **57** 603
21. Ghampson I T, Sepulveda C, Garcia R, Radovic L R, Fierro J L G, DeSisto W J and Escalona N 2012 Hydrodeoxygenation of Guaiacol over Carbon-supported Molybdenum nitride Catalysts: Effects of Nitriding Methods and Support Properties *Appl. Catal. A: Gen.* **439–440** 111
22. Sepulveda C, Leiva K, Garcia R, Radovic L R, Ghampson I T, DeSisto W J, Fierro J L G and Escalona N 2011 Hydrodeoxygenation of 2-methoxyphenol over Mo_2N Catalysts Supported on Activated Carbons *Catal. Today* **172** 232

23. de la Puente G, Centeno A, Gil A and Grange P 1998 Interactions between Molybdenum and Activated Carbons on the Preparation of Activated Carbon-Supported Molybdenum Catalysts *J. Colloid Interface Sci.* **202** 155
24. Shaheen W M and Selim M M 2002 Thermal Behaviour of Pure and Binary Basic Nickel Carbonate and Ammonium Molybdate Systems *Mater. Lett.* **52** 272
25. Vissers J P R, Bouwens S M A M, de Beer V H J and Prins R 1987 Carbon Black-supported Molybdenum Sulfide Catalysts *Carbon* **25** 485
26. Tien H -W, Huang Y -L, Yang S -Y, Hsiao S -T, Wang J -U, Ma C -C M 2011 Graphene Nanosheets Deposited on Polyurethane Films by Self-assembly for Preparing Transparent, Conductive Films *J. Mater. Chem.* **21** 14876
27. Lee J S, Lee K H and Lee J Y 1992 Selective Chemisorption of Carbon Monoxide and Hydrogen over Supported Molybdenum Carbide Catalysts *J. Phys. Chem.* **96** 362
28. Miura H, Osawa M, Sugiyuma K and Matsuda T 1986 The Adsorption of CO and Hydrogen on Reduced Molybdenum Catalysts Used for CO Hydrogenation *J. Catal.* **101** 178
29. Zaman S F, Pasupulety N, Al-Zahrani A A, Daous M A, Al-Shahrani S S, Driss H, Petrov L A and Smith K J 2017 Carbon Monoxide Hydrogenation on Potassium Promoted Mo_2N Catalysts *Applied Catalysis A: Gen.* **532** 133
30. Kumar P, Mungse H P, Cordier S, Boukherroub R, Khatri O P and Jain S L 2015 Hexamolybdenum Clusters Supported on Graphene Oxide: Visible-light Induced Photocatalytic Reduction of Carbon Dioxide into Methanol *Carbon* **94** 91
31. Li X, Feng L, Zhang L, Dadyburjour D B and Kugler E D 2003 Alcohol Synthesis over Pre-Reduced Activated Carbon-Supported Molybdenum-Based Catalysts *Molecules* **8** 13
32. Saito M and Anderson R B 1980 The Activity of Several Molybdenum Compounds for the Methanation of CO *J. Catal.* **63** 438